INSTITUTE OF PHYSICS PUBLISHING SEMICONDUCTOR SCIENCE AND TECHNOLOGY
Semicond. Sci. Technol. **18** (2003) 7–22 PII: S0268-1242(03)38249-5

High-bias current–voltage–temperature characteristics of undoped rf magnetron sputter deposited boron carbide (B_5C)/p-type crystalline silicon heterojunctions

M M Abdul-Gader Jafar

Department of Physics, Faculty of Science, University of Jordan, Amman 11942, Jordan

E-mail: mmjafar@ju.edu.jo

Received 17 June 2002, in final form 16 October 2002
Published 29 November 2002
Online at stacks.iop.org/SST/18/7

Abstract
The high-bias behaviour of the dark forward and reverse current–voltage (I–V) characteristics of an undoped radio frequency (rf) magnetron sputter deposited boron carbide (p-B_5C)/p-type crystalline silicon heterojunction has been investigated at different ambient temperatures (130–300 K). The experimental forward current–voltage–temperature (I–V–T) characteristics indicate that the non-ohmic bulk conduction mechanisms operable in the highly resistive polycrystalline B_5C counterpart material of this heterojunction largely determine the behaviour of its forward current at high-bias voltages (>0.3 V). The hopping conduction model of Apsley and Hughes for a flat density of localized energy states (Apsley N and Hughes H P 1975 *Phil. Mag.* **31** 1327) can be utilized to elucidate the bias dependence of the measured heterojunction forward current over an extended bias-voltage range (0.4–2.7 V) at temperatures below 260 K. On the other hand, the junction-like conduction processes occurring in the depletion region should limit the high-bias behaviour of the measured heterojunction reverse current. Bardeen's model for a modified Schottky-like barrier at the p-B_5C/p^+-Si interface can be satisfactorily applied to describe the reverse current–voltage characteristics at bias voltages larger than 0.4 V.

1. Introduction

Boron carbide is an important material in the fabrication of a wide variety of technological and electronic devices. Over the last two decades, considerable research has been made on the preparation and characterization of boron carbide films/alloys of different stoichiometric compositions and extrinsically doping materials [1–13]. Undoped boron carbide compounds are often categorized as p-type semiconductors though their energy-band structures are not yet fully established [9–13]. Nonetheless, the structures of boron carbide compounds, like other boron-rich solids, are supposed to have essentially high intrinsic defect concentration due to structural imperfections that often give rise to various localized states in the energy gap [11]. Further, among several other sophisticated preparation methods, the radio-frequency (rf) magnetron sputtering deposition (rf-MSD) method has been recently realized as a promising technique to fabricate high-quality semiconducting boron carbide ($B_{1-x}C_x$) films with controllable boron-to-carbon (B/C) ratio (composition x), and hence with selective optical and electrical properties [2]. The indirect energy-band gap width E_{g1} of undoped magnetron sputtered $B_{1-x}C_x$ films increases monotonically with the B/C ratio, whereas their electrical resistivity ρ decreases remarkably with increasing B/C ratio [2]. These two specific features make it highly possible to fabricate plausible rectifying heterojunctions composed of rf-MSD $B_{1-x}C_x$ films on moderately doped p-type ($p \approx 2 \times 10^{15}$ cm^{-3}) or n-type ($n \approx 1.4$–7×10^{14} cm^{-3}) crystalline silicon (c-Si) substrates of both (100) and (111) orientations [2]. Undoped boron carbide

films should thus have few free-charge carriers (holes) compared to the higher concentration of free-charge carriers (electrons/holes) existing in the counterpart n-/p-type c-Si substrates. Therefore, undoped $B_{1-x}C_x$/n-type c-Si and $B_{1-x}C_x$/p-type c-Si heterojunctions should, in principle, behave respectively as p–n and p–p^+ junction-like diodes, which in practice exhibit dissimilar current–voltage (I–V) characteristics depending on the B/C ratio of the $B_{1-x}C_x$ film used [1–8]. The magnetron sputter deposited p-B_5C/p^+-Si heterojunction is a typical example of such junctions that exhibits good electrical and heterojunction properties [2]. The B_5C material possesses a polycrystalline microstructure and has an optical dielectric constant ε_∞ of 7.5, a high absorption coefficient $\kappa \sim 10^5$ cm^{-1} in the visible spectrum, a large room-temperature (RT) electrical resistivity ($\rho_{RT} \sim 10^7\ \Omega$ cm) and E_{g1} (300 K) ~ 0.70 eV ($< E_{g1} \sim 1.1$ eV of c-Si) [2].

As reported in a quite recent work [3], the low bias (0–0.3 V) dark I–V curves of an undoped rf-MSD p-B_5C/p^+-Si (111) heterojunction exhibit a rectifying junction-like behaviour, but with an 'ideality factor' as large as 4 and suffer from large reverse currents, particularly at high temperatures. This has been attributed to the existence of high density of extrinsic interface states, formed throughout the fabrication procedure of the junction, and of intrinsic states caused by the lattice mismatch between the junction materials [14–19] and/or due to structural imperfections often existing in boron carbide compounds [2, 11]. The low-bias current transport in B_5C/c-Si heterojunctions has been described [3] satisfactorily by a model of the tunnelling of thermally excited carriers through the junction depletion region including tunnelling via impurity-localized states [20–22] over a broad temperature range (130–280 K). However, the high-bias behaviour of experimental forward and reverse I–V characteristics of rf-MSD B_5C/p-type c-Si heterojunctions differs remarkably from that observed at low biases. Traditionally, deviations from the expected junction-like forward I–V characteristics encountered at intermediate- and high-bias voltages are attributed to the so-called series-resistance effect, arising from the ohmic voltage drop across highly-resistive materials of the junction under study; so one can then modify the proposed rectifying junction model to include this effect [24–30]. However, the role of other effects giving rise to the observed deviations in the I–V characteristics of real junctions, such as front/back contacts to the junction, carrier tunnelling through narrow barriers at the hetero-interface regions, inherent bulk conduction in the junction materials, surface effects and high-injection levels, can in many cases be of paramount importance [18–37]. Motivated by this diversity in interpreting the observed high-bias I–V curves of practical junctions and by the need for more work on the transport properties of rf-MSD B_5C/c-Si heterojunctions, a detailed investigation of their experimental I–V–T characteristics at high-bias voltages is thus worthwhile. This would lead to further understanding the actual conduction mechanisms operating in these heterojunctions.

The present paper describes some measured dark dc I–V characteristics of an undoped rf-MSD deposited B_5C/p-type c-Si (111) heterojunction in a relatively broad bias-voltage range ($0 \rightarrow \pm 2.7$ V) at different ambient temperatures (130–300 K). The primary purpose of this paper is to elucidate the behaviour of the experimentally observed forward and reverse I–V–T characteristics of this heterojunction in the intermediate- and high-bias voltage regions using the existing electrical conduction models to determine the predominant charge transport mechanism(s) operable in this device.

2. Experimental details

The undoped p-B_5C/p-type c-Si (111) heterojunction used in the present study has a 60 nm thick B_5C film that has been fabricated by rf balanced magnetron sputtering deposition (rf-MSD) technique. The details of this rf-MSD method and the specific preparation conditions/procedures of the corresponding fabrication process are described elsewhere [2]. The sputtering deposition process of the B_5C films has passed through two separate working stages. The first stage was a pre-sputtering process in which a 'hydrogenated' B_4C source has been produced, where a 13.56 MHz magnetron sputter gun was used to drive a 1 Pa pressure mixture of argon (Ar) and methane (CH_4) glow discharge (plasma) at a relatively low rf power (<100 W) for several hours. The second stage is the actual sputtering process, in which the well-processed 'hydrogenated' B_4C source was then employed as a target for the deposition of B_5C films on the c-Si substrates, placed 7.5 cm from the target, which were chemically cleaned and etched prior to mounting on an electrically grounded aluminium holder being held at room temperature. This final rf magnetron sputtering deposition stage has been actually carried out in a pure argon plasma at a 0.8 Pa working pressure and a 100 W rf power. The composition (B/C ratio) of magnetron sputter deposited B_5C films has been maintained constant (within $\pm 5\%$) throughout the deposition period as determined from Auger electron spectroscopy (AES) studies. Oxygen levels were less than 2% atomic weight throughout a typical sputter deposited B_5C film [2].

A Van der Pauw technique has been utilized to measure the room-temperature bulk electrical resistivity of rf-MSD B_5C films deposited on quartz substrates using silver paste ohmic contacts on the top surface of the B_5C film [2]. The reported ρ_{RT} of rf-MSD B_5C films is as high as $10^7\ \Omega$ cm [2], which is lower than that reported for B_5C films produced by other deposition techniques [4–10]. Infra-red (IR) absorption measurements [2] made to characterize the quality of rf-MSD B_5C films revealed that, in addition to the presence of a substantial amount of carbon in these films, only a small content of hydrogen is usually present. The hydrogen bonding in the rf-MSD B_5C films usually exists in the form of a bridge structure, which is less stable than the hydrogen-bonding scheme found in B_5C films fabricated by other techniques [4–10]. Stable hydrogen bonding might lead to a dramatic reduction in the dangling carbon bonds in boron carbide films, and thus should play an important role in determining/limiting their electrical conductivity. Unfortunately, no numerical values of the hydrogen concentration in B_5C films were determined but based on the magnitude of the observed IR absorption peaks, only qualitative conclusions were reported [2].

Two thin copper electrical leads were attached to contact spots (~3 mm in diameter) of a conducting-silver paste placed on front and back surfaces of the present B_5C/p-type c-Si

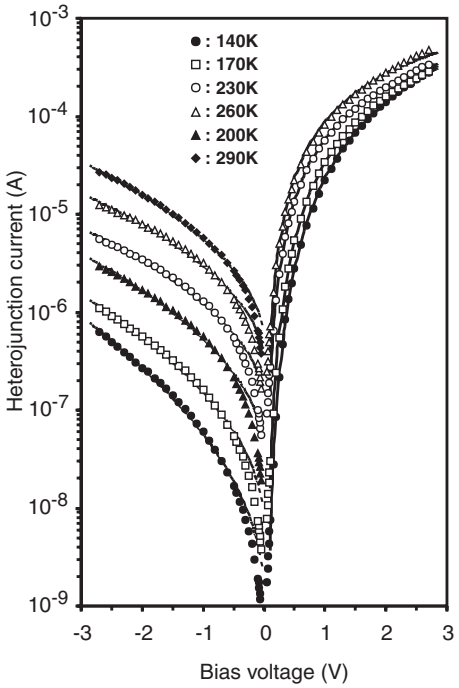

Figure 1. Typical experimental forward- and reverse-bias dark current–voltage (*I–V*) characteristics of the undoped rf magnetron sputter deposited B_5C/p-type c-Si heterojunction device used in this work at different ambient temperatures represented by the symbols shown. The solid- and dashed-line curves depict the forward- and reverse-bias *I–V* curve fits obtained as described in figures 8 and 10.

junction to form an electrical sandwich configuration cell. For this junction, which resembles a p–p^+ heterojunction structure, the forward current was measured when a negative bias is connected to the p-side of the junction (i.e., to the undoped p-B_5C layer) [2, 3]. The ambient temperature T of the cold finger of a He-type closed-cycle cryostat, to which the junction cell was thermally anchored, was varied in the range 130–300 K, over which temperature settings were controlled and maintained steady to better than (±0.5 K). Current measurements on the present B_5C/p-type c-Si device were carried out, at a fixed T, under dark vacuum environment using a Keithley 614 electrometer as a function of positive and negative dc bias voltages in the range 0–2.7 V (±0.5%). The current readings were reasonably stable and reproducible within an uncertainty better than ±10%, even in the lowermost pico-ampere ranges of the electrometer.

3. Experimental results

Figure 1 shows a typical set of experimental forward and reverse dark current–voltage (*I–V*) curves of the investigated rf-MSD p-B_5C/p^+-type c-Si heterojunction device for dc bias voltages in the region 0–2.7 V at different ambient temperatures (130–300 K). The measured forward semi-log *I–V* characteristics exhibit a remarkably non-linear behaviour at intermediate-/high-bias voltages, with relatively weak current–temperature dependence. Further, these forward *I–V* curves tend to coalesce at the highermost bias-voltage side at low temperatures, where the forward current seems to become less dependent on temperature. The corresponding isothermal

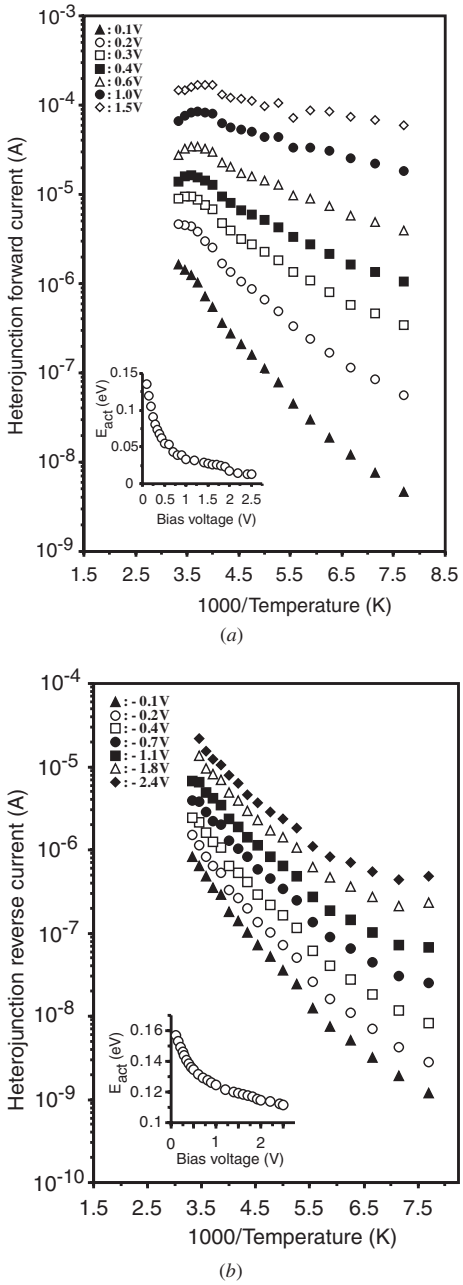

Figure 2. The temperature dependence of the measured heterojunction current ($I(V, T)$) on semi-log ($I(V, T)$,) versus $1000/T$ (K) curves (Arrhenius plots) at different bias voltages for (*a*) the forward-bias case and (*b*) the reverse-bias case. The insets show the bias-voltage dependence of the 'activation' energy E_{act} deduced from the obtained best curve fits of the appropriate linear segments falling on the corresponding experimental curves to the formula ($I(V, T) \propto \exp[-E_{act}/k_B T]$.

reverse *I–V* curves are well apart over the whole bias-voltage range studied and show much less non-linearity (or bending) with bias, with the reverse-current values being much lower than those of the forward current at the same bias voltage and temperature.

Figures 2(*a*) and (*b*) depict the temperature dependence of the measured current of the heterojunction device, represented by semi-log I versus $1000/T$ curves (i.e., the current–temperature Arrhenius plots) at different forward- and

reverse-bias voltages between 0 and 2.7 V. The forward $\ln I$ versus $1000/T$ curves appear to exhibit a thermally activated (Arrhenius) behaviour, but over a rather narrow temperature range, with deviations from this Arrhenius behaviour at low temperatures. In addition, at bias voltages $\geqslant$0.2 V, these forward $\ln I$ versus $1000/T$ curves clearly exhibit some sort of peaks in the high-temperature region (around 280 K). The Arrhenius plots of the reverse current show a visual linearity over a relatively wider temperature range, though these curves gradually deviate from this Arrhenius linearity with decreasing temperature. The slope of the best linear portions (i.e., the activation energy E_{act}) of the forward-current Arrhenius plots was noted to decrease dramatically with increasing bias voltage (see inset to figure 2(*a*)), whereas the slope of these linear parts of the reverse-current Arrhenius plots decreases slightly with the bias voltage (inset to figure 2(*b*)). An analysis of the activation energy-bias data deduced from the forward- or reverse-current–temperature Arrhenius plots showed that no specific physically meaningful voltage dependence of E_{act} could be assigned to the whole bias-voltage range studied, though some sort of a $V^{1/2}$ dependence may be obtained, but over a limited bias range.

However, the distortions of the Arrhenius linearity seen in the forward $\ln I$ versus $1000/T$ plots of the present p-B_5C/p^+-c-Si heterojunction disappear upon re-plotting the same forward *I–T* data, at a fixed bias, as $\ln IT^{1/2}$ versus $T^{-1/4}$. At forward-bias voltages above 0.2 V, these plots plausibly fall on 'visibly good' straight lines only over the temperature range 130–270 K as depicted in figure 3(*a*), which, however, exhibits a $T^{-1/4}$ dependence of the heterojunction current fairly well over a broader temperature range at lower biases. The high-bias reverse $\ln IT^{1/2}$ versus $T^{-1/4}$ plots exhibit a weaker bias-dependent linearity in the high-temperature region, with noticeable deviations from this linearity at low temperatures, as seen in figure 3(*b*). Only, the slope, B_M (in $K^{1/4}$), of the 'visibly good' straight-line portions falling on the measured forward-bias $\ln IT^{1/2}$ versus $T^{-1/4}$ plots decreases progressively with increasing forward-bias voltage. This implies that the high-bias conduction processes in the reverse case differ from those giving rise to the high-bias forward-current behaviour. Figures 4(*a*) and (*b*), however, demonstrate that the same forward- and reverse-bias *I–T* data also yield a 'visibly good' linear trend on $\ln I$ versus $T^{1/3}$ plots with the same sort of bias dependence of their slopes $G(V)$, as seen in the corresponding insets.

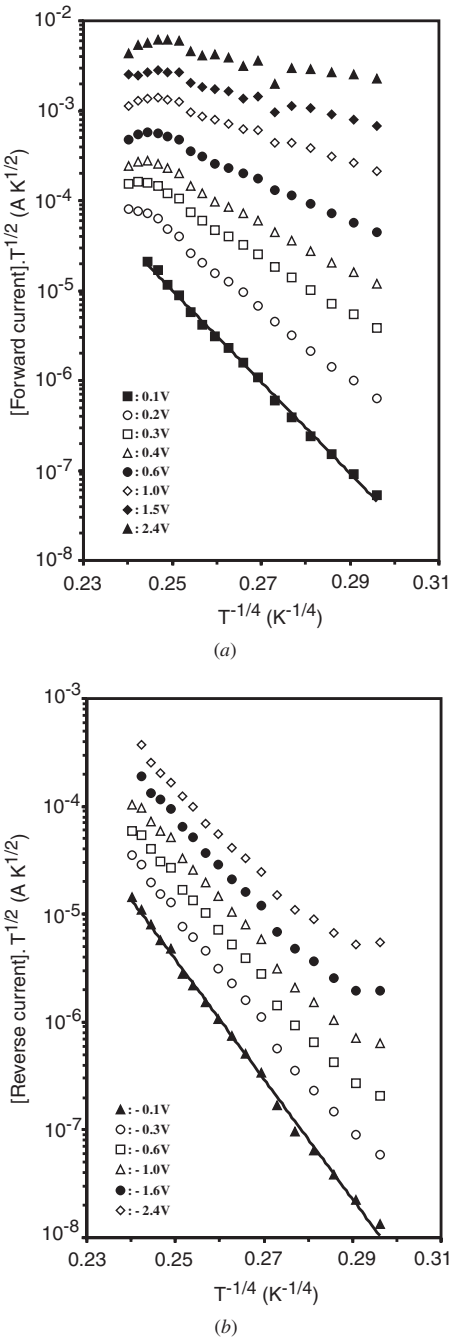

Figure 3. The measured heterojunction current data re-plotted at different bias voltages as $\ln IT^{1/2}$ versus $T^{-1/4}$ for (*a*) forward and (*b*) reverse bias. The symbols and solid lines (at $\pm$0.1 V) represent respectively the measured data and curve fits to a Mott-like hopping formula $I(V, T) \propto T^{-1/2} \exp[-C(V)/T^{1/4}]$.

4. Analysis and discussion of results

The above-described behaviours of the experimentally observed forward and reverse currents of the undoped p-B_5C/p^+-type c-Si heterojunction investigated in the present work with bias voltage and temperature reveal, at least, two main important features. Firstly, the conduction phenomena responsible for the forward-bias current of this heterojunction device are seemingly different from the conduction processes giving rise to the behaviour of its reverse-bias current at intermediate- and high-bias voltages. Secondly, the heterojunction forward-bias current behaviour in the high-temperature region (>270 K) is not the same as observed at lower temperatures. An intensive analysis of the measured *I–V–T* data of this heterojunction has been thus carried out to identify the predominant charge transport mechanism(s) giving rise to the observed high-bias current behaviour with bias and temperature.

Assuming that the junction depletion region still limits the device electrical behaviour, the experimentally observed deviation of its forward-current behaviour at high-bias voltages from the *I–V* characteristics of a diode-like junction in the low-bias regime can be explained in terms of a series-resistance (R_s) effect, which may remarkably modify the actual rectifying

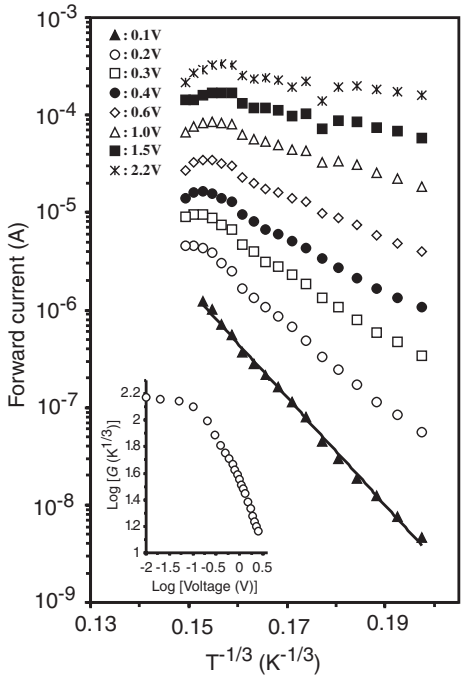

(*a*)

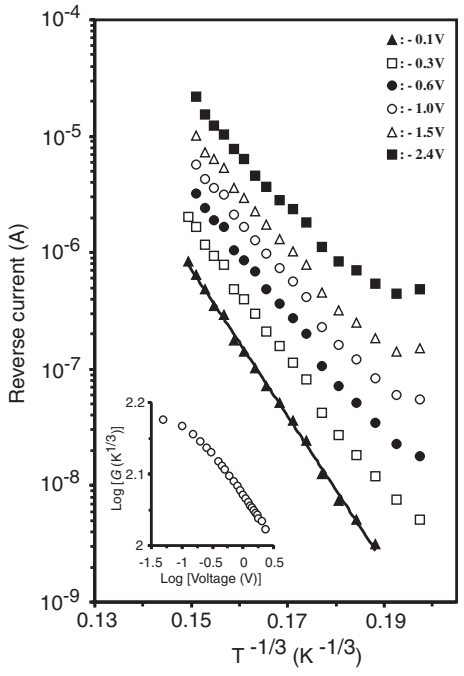

(*b*)

Figure 4. The current–temperature data of figure 3 are re-depicted at different bias voltages on $\ln I$ versus $T^{-1/3}$ curves for (*a*) forward and (*b*) reverse bias. The symbols and the solid lines (at ± 0.1 V) represent respectively the measured data and curve fits to the formula $I(V,T) \propto \exp[-G(V)/T^{1/3}]$. The insets show the bias dependence of the 'gradient' $G(V)$ deduced from the corresponding best curve fits.

junction-like behaviour at high-bias voltages. An ohmic voltage term IR_s is usually included in the diode-like formula to account for such a series-resistance effect [16, 24–30]. One can then employ a workable and reliable curve-fitting technique [4, 38–42] to obtain physically reasonable fits of the measured forward *I–V* curves over the desired bias-voltage region to such a modified non-linear junction model in order to extract the junction parameters of interest. Alternatively, other workers have applied graphical/non-graphical analytical approaches that utilize specifically formulated empirical auxiliary functions to analyse the series-resistance limited *I–V* characteristics of junctions on the basis of such modified diode-like formulae [26, 27]. In practice, however, such data-analysis approaches may not be always appropriate and often involve certain limitations or unrealistic results [3, 27]. In addition, the numerical/graphical analysis of the *I–V–T* data of a real junction would become rather complicated or less physically informative if bulk conduction phenomena in the junction materials largely mask the actual junction-like behaviour, particularly when at least one of its materials has a high temperature-/voltage-dependent inherent resistivity. In principle, the effect of bulk conduction in a junction having a highly resistive semiconducting layer becomes important in a junction at high-bias voltages in the forward-bias direction and not in the reverse-bias case, where a rectifying junction-like behaviour should be dominant [36, 37]. This seems also plausible in the p-B_5C/p^+-type c-Si heterojunction used in the present work, as its rf-MSD undoped polycrystalline B_5C counterpart film possesses a relatively large electrical resistivity even at high temperatures [2, 3]. Further, experimentally observed departures from the diode-like behaviour of a real junction in the high-bias regime and the consequent additional complication of a reliable analysis of its measured *I–V–T* data may also result from other conduction mechanisms related to the existence of some insulating interfacial layer, recombination–generation processes in the depletion region and high-injection levels [28–30].

The experimental isothermal *I–V* results in general can be treated using an empirical relation of the form $I(V,T) \sim \exp(eV/\eta k_B T)$, with the ideality diode factor η being in the range 1–4, depending on the actual processes dominating the conduction in the junction [3, 16, 28–30, 37]. Careful inspection of the measured *I–V–T* curves of the present heterojunction revealed that the behaviour of its forward current at intermediate- and high-bias voltages (>0.3 V) cannot be reliably analysed using such an empirical formula even when it was modified by the incorporation of a series-resistance effect, but over a limited narrow bias region. This suggests that conduction processes occurring in the highly resistive counterpart polycrystalline B_5C material of this p-B_5C/p^+-type c-Si heterojunction would be a possible alternative candidate in determining its forward current in the intermediate-/high-bias regimes. Therefore, in the following discussion, the possible current conduction mechanisms that would be operable in an undoped polycrystalline semiconducting B_5C film will be explored to achieve some further understanding of the behaviour of the measured forward current–voltage characteristics of this heterojunction in the voltage region beyond that of the low-bias diode-like behaviour. On the other hand, the experimental reverse current–voltage characteristics of such a heterojunction indicate that the junction depletion region itself does limit its reverse-bias current, and the appropriate rectifying junction-like formulae were thus employed to examine its reverse *I–V* curves.

4.1. High-bias current conduction mechanisms in undoped rf-MSD p-B_5C/p^+-type c-Si heterojunctions in the forward direction

Among all possible conduction processes operable in a solid beyond the ohmic (low-field) regime, the Schottky-emission process, Poole–Frenkel effect, space-charge-limited-current (SCLC) conduction and non-ohmic hopping conduction are well-known mechanisms [17–23, 31–37, 43–57] that could determine the high-bias forward current in a junction having a semiconducting layer as one of its counterparts. To examine which of these charge transport mechanisms were responsible for the measured high-bias forward *I–V–T* characteristics of the present undoped rf-MSD p-B_5C/p^+-type c-Si heterojunction, one should test the applicability of the theoretical models describing these conduction mechanisms. The mathematical rigour of these models are briefly presented in appendices A, B and C.

4.1.1. Poole–Frenkel and Schottky-type conduction mechanisms. Analysing the high-bias forward *I–V–T* characteristics of the present rf-MSD p-B_5C/p^+-type c-Si heterojunction on the basis of the simple Schottky-type and Poole–Frenkel formulae given in appendix A showed that the usual isothermal semi-log I or (I/V) versus $V^{1/2}$ plots exhibit reasonably good linear portions but over a rather narrow high bias-voltage range. Therefore, because of such limited-range portions of these plots and the lack of auxiliary and complementary measurements [22, 32, 44–48], no further analysis of these characteristics was made [22, 31, 32] to test the possibility of Schottky-type and/or Poole–Frenkel conduction mechanisms in the present heterojunction. Further, an in-depth analysis of these forward *I–V–T* data on the basis of the comprehensive theories and analytical normalization procedures describing the so-called single- and multiple-centre Poole–Frenkel emission mechanisms in solids [20, 54] showed that such conduction mechanisms cannot be the main candidate for the experimentally observed forward-current behaviour over the whole intermediate-/high-bias-voltage regimes studied.

4.1.2. SCLC conduction. Re-analysing the same experimental forward *I–V–T* data of the B_5C/c-Si heterojunction device used in the present work on the basis of the commonly accepted SCLC conduction formulae described in appendix B revealed a poor representation of the measured heterojunction high-bias forward current in terms of a SCLC mechanism operating in the presence of uniformly distributed traps. On the other hand, the isothermal log–log *I–V* plots exhibit reasonably good visual linearity over a relatively wide bias-voltage range (0.5–2.1 V) at temperatures below 260 K as depicted in figure 5. The inset to figure 5 demonstrates the temperature dependence of the parameters $m(T)$ and $K(T)$ of the general SCLC equation (B4), as reported in other devices [34–37]. For temperatures above 240 K, the range of the $m(T)$ values of the reasonably good linear portions of the corresponding isothermal forward log–log *I–V* curves lies between 1.7 and about 2. This may be tentatively presumed to represent a nearly Mott–Gurney V^2 behaviour, which should be expected in the case of space-charge currents limited by discrete shallow traps or for trap-free limited SCLC conduction (appendix B). However, the nature of the forward-bias current variation with temperature beyond a current peak around 270 K is seemingly arising from a non-activated weak conduction mechanism due to scattering by thermal lattice vibrations, for which the trap-limited mobility μ of the material should decrease with temperature T and electric field F roughly as $\mu \propto F^{-1/2}T^{-3/2}$ [23]. One can thus understand the observed bias dependence of this experimentally observed high-temperature forward current by combining this mobility field dependence with the V^2 dependence of the shallow-trap SCLC process.

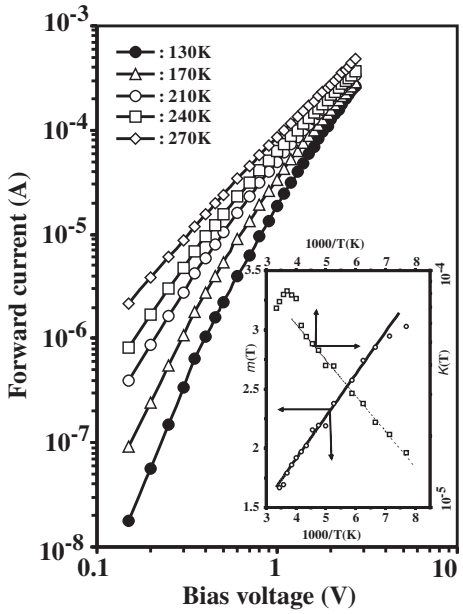

Figure 5. Typical isothermal log $[I(V,T)]$ versus log V plots for the experimental forward-bias current data (symbols). The solid lines are just a guide to the eye. The inset shows the temperature dependence of the 'exponent' $m(T)$ and the pre-factor $K(T)$ deduced from the best curve fits of reasonably selected linear portions of log *I*–log*V* plots to the SCLC formula $I(V,T) = K(T)V^{m(T)}$, with the solid and dashed lines representing respectively the best fits to $m(T) - 1 = 260\ \mathrm{K}/T$ and $K(T) \propto \exp[-0.03\ \mathrm{eV}/k_\mathrm{B}T]$.

At lower temperatures down to 130 K, however, the exponent $m(T)$ increases with decreasing temperature up to a value of 3, as expected for SCLC conduction [34–37]. Thus, at first glance the reasonably observed $V^{m(T)}$ dependence of the forward-bias current of the present undoped p-B_5C/p^+-c-Si heterojunction can lead one to conclude that trap-limited space-charge currents in the B_5C layer are probably dominating its forward-bias current transport at bias voltages beyond the low-bias junction-like regime. This may sound plausible, as a pseudo-Schottky contact [48] could exist at the B_5C/c-Si interface of this heterojunction. Hence, a continuous supply of injected charge carriers (holes) can proceed through the junction from the moderately doped crystalline p^+-Si ($p \sim 2 \times 10^{15}\ \mathrm{cm}^{-3}$) into the 'extrinsically' undoped highly-resistive polycrystalline p-B_5C material with much lower concentration of free holes to sustain flow of trap-limited space-charge currents. But, the relatively too low activation energy E_act (∼0.03 eV) deduced from the slope of the $K(T)$ versus $1/T$ plot in the region 140–250 K cannot be reliably

interpreted as the minimum energy for a charge carrier to be thermally emitted from an ionizable impurity or a trap state near the Fermi level to the semiconductor energy band involved [34–37]. Instead, other charge transport mechanisms should give rise to the forward-bias current of this heterojunction such as thermally-assisted tunnelling-like/hopping conduction that could be operable in a material [20–22, 49–57].

4.1.3. Thermally- and field-assisted tunnelling-like/hopping conduction. Traditionally, the low-temperature current transport in semiconducting materials with too low activation energies (i.e., a few meV) is related to hopping of charge carriers between densely distributed energy states in a localized energy region within the material energy gap [20–22, 32, 49–57]. Appendix C summarizes the physical features and formulation of the different hopping/tunnelling-like conduction mechanisms that can determine the conductivity (current) of a semiconducting specimen in both ohmic (i.e., low field) and non-ohmic regimes. It is worth noting here that the term 'low temperature' should not be considered literally, as the temperature region in which hopping/tunnelling-like conduction takes place usually varies from one material or a junction device to another [3, 12, 13, 20–22, 49–57].

There is experimental evidence showing that hopping conduction predominates the charge transport in boron carbides in the ohmic region in the temperature range 4.2–300 K; however, the proposed hopping mechanisms and the corresponding theoretical models used to interpret the low-field conductivity–temperature data are still controversial issues [12, 13]. The presence of high-density localized states in real boron carbides or boron carbide based heterojunctions, partly due to the intrinsic defect concentration caused by structural imperfections and broken dangling bonds and partly due to interface states that could form through the fabrication of junctions, is expected. Such a large density of localized energy states would make hopping/tunnelling-like conduction highly possible to occur, and probably to be the dominant transport mechanism, in boron carbide compounds over a wide range of temperatures. The experimentally observed low-bias voltage–current–temperature characteristics of an undoped rf-MSD B_5C/p-type c-Si heterojunction were satisfactorily described [3] by a thermally-assisted tunnelling conduction model of the $T^{-1/3}$ dependence [20, 21] over the temperature range 130–280 K. Moreover, the 'visually good' and indistinguishable linear $T^{-1/3}$ and $T^{-1/4}$ behaviours of the forward-bias current of the present B_5C/p-type c-Si heterojunction depicted in figures 3 and 4 can also be taken as a further evidence for the occurrence of three-dimensional (3D) hopping/tunnelling conduction in its undoped rf-MSD B_5C material film. Actually, the same *I–T* data at any fixed forward bias of this heterojunction were noted to exhibit also 'visually good' linear $\ln I \propto T^{-1/7}$ plots.

Indeed, the same measured conductivity– (current) temperature data of a semiconductor may exhibit, within experimental error, 'visually good' and indistinguishable linearity on the $\ln\sigma$ (T) versus $T^{-1/n}$ plots for any n value ($n = 2$, 3, 4 or 7) over the temperature range covered, though each n characterizes a different hopping/tunnelling-like conduction mechanism [20, 32, 53]. This form of plot by itself, then, will be insufficient evidence for defining any one of these hopping/tunnelling-like conduction mechanisms to identify the behaviour of the experimental sample current/conductivity. Thus, skilful intuition in addition to experimentally deduced physically meaningful values of the parameters involved in theoretical models describing these charge transport mechanisms would allow one to distinguish between them and thereby justify which conduction process should dominate the observed conductance behaviour [20, 32, 49–57]. Alternatively, another approach often utilized to achieve some real characterization of the predominant hopping/tunnelling-like mechanism in semiconducting materials is to examine the electric field dependence of their conductance over a rather wide range of temperature and field [20, 49–56].

A 3D $T^{-1/2}$-hopping behaviour of the forward-bias current of the present B_5C/c-Si heterojunction should only be observed at temperatures far below the temperature range studied here [49–57]. Further, the reported analytical formulation of the hopping conduction model that treats the case of charge-carrier hopping from ionizable centres into traps, which gives rise to a conductivity–(current) $T^{-1/7}$ dependence, is only for the low-field case [20]. No detailed analytical formulation on the field dependence of the variable-range trap hopping (VRH) conductivity $T^{-1/3}$ law expected in 2D structural systems is also available [22, 49]. Therefore, no more analysis of the measured *I–V–T* data of the present heterojunction in view of these hopping conduction mechanisms will be carried out in this work.

However, a $T^{-1/3}$ dependence of a field-dependent dc conductivity (current) has been predicted for thermally-assisted tunnelling of charge carriers through a field-reduced Poole–Frenkel barrier of an ionizable impurity centre into a quasi-conduction band, which has been justified in some semiconducting heterojunctions [3, 20, 21]. The experimental *I–V–T* curves of the present B_5C/c-Si heterojunction were in fact thoroughly analysed in accordance with equation (C1) of this model (see appendix C) and the results are depicted in figure 6, where a reasonably good agreement between theory and experiment can be noted in the forward-bias voltage range above 0.6 V. The theoretical (solid) curves of figure 6 were obtained using a 'simulation' curve-fitting procedure [3, 16], where a 'visual' control of the adjustable fitting parameters within a physically reasonable range and a realization of cases in which the 'model' curve could not critically match the measured data are often achieved. It has been realized that values of the adjustable energy parameter E_p around 0.1 eV and an effective thickness $d^* \sim 10$ nm, which is less than the physical thickness of the B_5C film of the heterojunction, were selected to obtain physically meaningful and reliable 'fit curves'. The small peak energy of the Poole–Frenkel reduced barrier of ionizable centres is not unrealistic, while the low value of thickness could be related to electric-field non-uniformity due to the accumulation charge layers in the film and/or at the B_5C/Si interface [31–34]. Further, a plot of the gradient $G(V)$ of the forward-bias $\ln I$ versus $T^{-1/3}$ plots against $V^{-2/3}$ yields a good linear part in conformity with equation (C1), but over a narrow bias range as seen from the inset to figure 4(*a*). The deviation from the expected straight-line dependence of $G(V) \propto V^{-2/3}$ can be accounted for by including the second term of equation (C1), which should

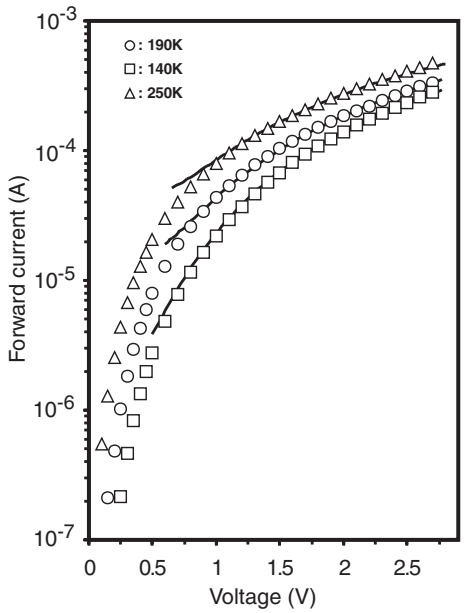

Figure 6. Typical isothermal $\ln I$ versus V curves of the measured forward-current data (symbols). The solid curves are simulation fits of equation (A8) to the data above 0.6 V, with $E_p \sim 0.1$ eV and $d^* \sim 10$nm.

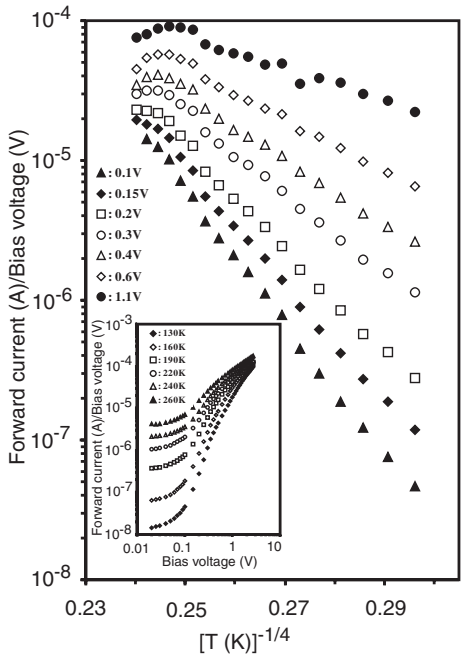

Figure 7. The temperature dependence of the experimental forward-bias junction conductance (I/V) plotted as $\ln[I/V]$ versus $T^{-1/4}$ at different bias voltages. The inset depicts the same data on $\ln[I/V]$ versus $\ln V$ plots at different temperatures.

become important at high bias voltages. The tendency of the gradient $G(V)$ to level off at the low bias-voltage side is also expected because the parameter E_0 tends to approach the value of E_p at low fields, as predicted by this conduction model [20]. These findings suggest that Hill's $T^{-1/3}$ model describing thermally-assisted tunnelling through a field-lowered Poole–Frenkel barrier [20, 21] can reasonably describe the measured high-bias forward current of the present heterojunction, at least in some range of temperature and voltage, despite the fact that the existence of ionizable centres in its undoped B_5C counterpart material may not be wholly justified. However, the presence of 'intrinsic' defects due to 'inherent' structural imperfections in real boron-rich systems [11] and the inclusion of 'native' impurities during the fabrication process of rf-MSD B_5C films [2] are both possible.

As the existence of a large density of localized intrinsic/extrinsic energy states and traps is probable in rf-MSD B_5C films, hopping conduction among these localized states would be more plausible. The applicability of Hill's $T^{-1/4}$ 'trap hopping' conduction model for the case of uniformly/exponentially distributed localized trap energy states, described in appendix C, to the measured forward-bias current data of the present B_5C/c-Si heterojunction was first examined using the normalization current–temperature–field characterization procedure and the related formulae [20]. However, the results obtained (not given here) were not conclusive and showed a less satisfactory agreement between theory and experiment even in a narrow bias-voltage range. In this context, the forward-bias current data of the present heterojunction cannot also be explained in view of hopping conduction theories in which $\sigma(F,(T) \propto \sigma(0,T)\exp[eFL/k_BT]$, where $\sigma(0,T)$ is the zero-field hopping conductivity ($\ln\sigma(0,T) \propto T^{-1/4}$) and L is a maximum hop length [49, 53].

Finally, the Apsley–Hughes hopping conduction model, which describes the temperature and field dependence of VRH hopping conduction for the case of a flat density of localized energy states [55], has been adapted to analyse the measured forward-bias I–V–T data of the same B_5C/c-Si heterojunction. As described in appendix C, the Apsley–Hughes hopping conduction model, as all other field-dependent hopping theories, yields the 3D VRH Mott-like $T^{-1/4}$ dependence of the ohmic conductivity at sufficiently low electric fields for which $\beta = [eF/2\alpha k_BT] \leqslant 0.1$. In fact, the $T^{-1/4}$ trend is exhibited in the semi-log forward conductance (I/V) versus $T^{-1/4}$ curves of the present heterojunction at any bias voltage over a wide temperature range (130–270 K) as shown in figure 7. The inset to figure 7 shows that the conductance of the heterojunction tends to become entirely field dependent and temperature independent at high bias voltages, while its behaviour at the low-bias side shows strong temperature and weaker bias dependences, which can be compared with the calculated results of Apsley and Hughes [55]. This suggests that one can utilize the hopping conduction model of Apsley and Hughes to describe the forward-bias current of this B_5C/c-Si heterojunction, as VRH hopping conduction mechanism seems to be operable in its semiconducting rf-MSD B_5C counterpart material, in which intrinsic/extrinsic localized energy states do exist. The deduced values of the slope $C(V)$ of the reasonably good straight lines falling on the measured low-bias $\ln(I/V)$ versus $T^{-1/4}$ plots are remarkably high, tending to be slightly bias dependent at the lowermost forward-bias voltages. For example, $C(V) \sim 109\,K^{1/4}$ at a forward voltage of 0.1 V, corresponding to Mott's localization temperature T_M as high as 10^8 K, which might be related to a high degree of disorder/structural imperfections in the material [49, 57]. Using a

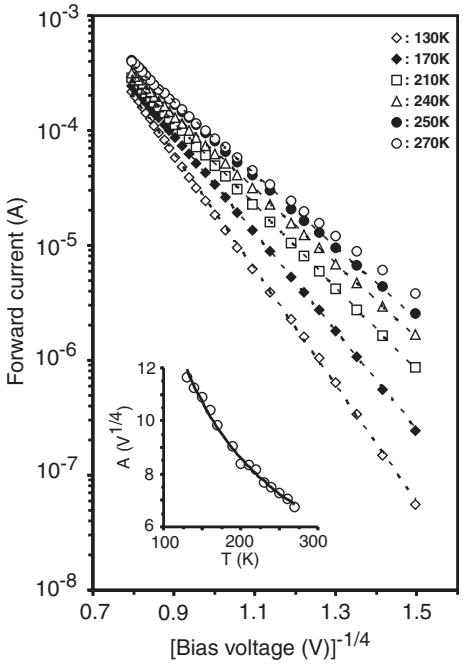

Figure 8. Typical isothermal forward-bias $\ln I$ versus $V^{-1/4}$ curves, where the symbols and dashed lines represent respectively the measured data and their curve fits to the formula $I(V, T) \propto \exp[-A(T)/V^{1/4}]$. The inset illustrates the deduced temperature dependence of the 'gradient' $A(T)$ of these fits (circles), with the solid line depicting the relation $A(T) \propto T^{-0.77}$.

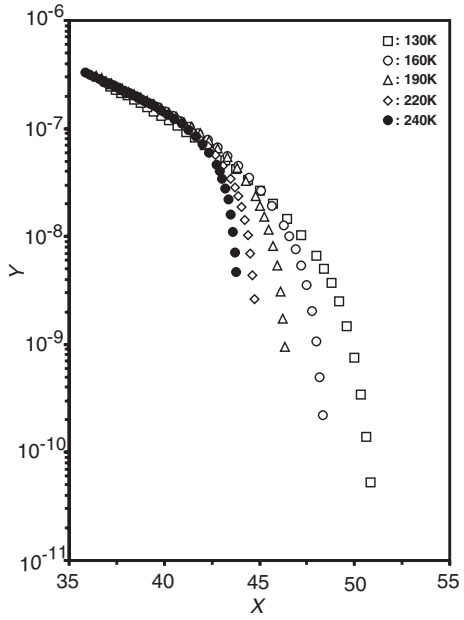

Figure 9. The heterojunction forward-bias current–voltage–temperature characteristics plotted according to the Apsley–Hughes hopping conduction theory [55]. In this plot, the forward-bias voltage and current ranges used are 0.1–2.7 V and 10^{-9}–10^{-4} A at the temperatures shown. The Y values are the ratio Id^*/V divided by the four pre-exponential factors in equation (A13) and the X values are the exponential argument in the same equation. The values of the parameters yielding these results are $S = 0.07$ cm^2, $\alpha = 10^7$ cm^{-1}, $d^* = 3 \times 10^{-6}$ cm, $N = 10^{17}$ eV^{-1} cm^{-3} and $\nu_{ph} = 10^{13}$s^{-1}.

decay constant α of 10^7 cm^{-1}, the low-bias $C(V)$ values give rise to a large density of localized energy states $N \sim 6 \times 10^{17}$ eV^{-1} cm^{-3}, which sounds quite reasonable in the case of boron carbides such as the rf-MSD undoped B_5C polycrystalline films. However, even at the low-temperature side available, figure 7 does not show explicitly the expected deviation from the conductivity/current $T^{-1/4}$ behaviour with increasing bias voltage [55]. The field-dependent hopping conductivity regime, where the conductance should become temperature insensitive [49–56], as the Apsley–Hughes theory clearly predicts [55], would, however, be reached if reliable and reproducible measurements of the heterojunction forward-bias current were possible in the range of low temperatures wider than that reported here.

As a further check of the applicability of the Apsley–Hughes hopping conduction model [55] to the measured forward-bias *I–V–T* data of the present heterojunction, these data were re-presented on isothermal semi-log current versus $V^{-1/4}$ plots, as shown in figure 8, which shows remarkably linear curves over the entire bias-voltage region 0.4–2.7 V, particularly at temperatures below 260 K. As the bias voltage is decreased below 0.4 V these $\ln I$ versus $V^{-1/4}$ curves deviate from the $V^{-1/4}$ linearity and this, of course, could be related to a junction-like behaviour [3] rather than to the hopping conduction mechanism in the B_5C layer of the heterojunction. Similar presentation of the same data on isothermal semi-log current versus $V^{-1/n}$ plots based on other theoretically grounded values of n (=1, 1.5, 2) [20, 49, 53] was also made, but those plots did show strong deviations from a too limited linearity as the bias voltage decreases. Further, the family of isothermal linear $\ln I$ versus $V^{-1/4}$ plots tends to merge at the highermost biases, implying that a temperature-independent conductance could be observed at much higher forward-bias voltages. At low-/intermediate-bias voltages, however, the temperature dependence of such highly linear forward-bias $\ln I$ versus $V^{-1/4}$ plots is appreciable, with their slopes being noted to follow a $T^{-0.77}$ trend, as seen in the insert to figure 8. This temperature dependence of such a deduced slope cannot be understood from the hopping conduction theory of Apsley and Hughes. Nonetheless, these findings still suggest that a VRH conduction in the highly resistive B_5C layer is probably an important current mechanism that should determine the heterojunction forward-bias current over a wide bias-voltage range and this VRH mechanism can be described, at least qualitatively, by the Apsley–Hughes hopping conduction model [55].

In fact, the general Apsley–Hughes hopping conductivity equation (C6), in spite of its complexity, gives the possibility to plot the forward-bias current–voltage–temperature data of the present heterojunction at one time without considering the two asymptotic regions at low and high electric fields [56]. Figure 9 exemplifies such a plot, which shows that the high-bias forward *I–V–T* data of the present B_5C/c-Si heterojunction at different ambient temperatures tend to distribute over one single straight line, as expected from the Apsley–Hughes theory [55], and as reported for other high-resistivity semiconducting materials [56]. In fact, the isothermal curves of the general plot of figure 9 has been obtained by assuming $N = 10^{17}$ eV^{-1} cm^{-3}, $\alpha = 10^7$ cm^{-1}, a sample thickness $t = 3 \times 10^{-6}$ cm and $\nu_{ph} = 10^{13}$ s^{-1}. These results suggest that one can successfully utilize the

Apsley–Hughes conduction model to describe the temperature-/bias-voltage dependencies of the forward-bias current of the present heterojunction in the temperature range studied at bias voltages higher than 0.3 V. However, figure 9 shows that the experimental I–V–T data deviate from the linear trend expected from the Apsley–Hughes hopping model at low-bias voltages towards lower conductance (current) values, a feature that has been reported to be peculiar to high-resistivity semiconducting samples, as no such deviations should be observed at any electric field for less resistive compounds [56]. Thus, such an observed discrepancy has been partly related to correlation effects in such high-resistivity samples due to the existence of collective charge-carrier energy states produced by the carrier–carrier interaction, leading to a correlated hopping transport, for which a one-particle hopping model such as the Apsley–Hughes one should be inappropriate [56]. This could also be true in the case of the B_5C/p-type c-Si heterojunction if its forward-bias current at these bias voltages is assumed to be governed by hopping conduction in its highly-resistive polycrystalline B_5C material. Alternatively, however, one can attribute the observed deviations seen at low forward-bias voltages in this general plot of the current data of this heterojunction to different current conduction modes arising from the emission-limited conduction phenomena occurring in the junction depletion region itself [3, 28, 29].

4.2. High-bias charge transport mechanisms in undoped p-B_5C/p^+-type c-Si heterojunctions in the reverse direction

Figures 1–4 show that the measured forward- and reverse-bias current–voltage–temperature characteristics of the B_5C/p-type c-Si heterojunction studied in the present work are dissimilar, at least in two major respects. First, the reverse-current levels are much lower than the forward-current values at the same ambient temperature and bias voltage. Second, the behaviour of the reverse current with temperature and bias voltage in the high-bias region (>0.4 V) is seemingly of different conduction origin compared with the conduction mechanisms giving rise to the bias/temperature dependence of the forward current. Indeed, an analysis of the bias/temperature dependence of the measured heterojunction reverse current on the basis of the several bulk conduction models already used in analysing its forward-current behaviour has been found to give a less satisfactory interpretation of the overall high-bias reverse-current behaviour. Therefore, the measured high-bias reverse current is more likely to be governed by the actual junction-like behaviour via the charge transport mechanisms operable in the heterojunction depletion region. This junction-like behaviour is exemplified clearly in the isothermal semi-log reverse-bias current versus $V^{1/2}$ plots, where a 'visually remarkable' linearity can be noticed over a broad reverse bias-voltage range ($\sim$0.5–2.7 V) at almost all ambient temperatures studied as depicted in figure 10. In the present rf magnetron sputter deposited p-B_5C/p^+-type c-Si heterojunction, this may be understood in terms of a Schottky emission over a pseudo-Schottky-contact barrier [48] that could be presumably formed at the Si/B_5C interface, where injection of free-charge carriers (holes) from the moderately doped crystalline silicon into the 'extrinsically undoped' B_5C film layer would occur.

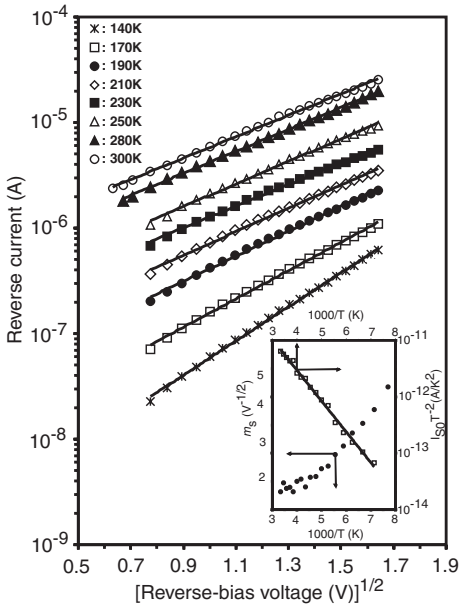

Figure 10. Typical isothermal semi-log plots of the measured junction reverse-bias current versus $V^{1/2}$, with the solid lines depicting the best fits to $I_S(V,T) = I_{S0}(T)\exp[m_S(T)V^{1/2}]$. The inset shows the temperature dependence of the deduced $I_{S0}(T)$ (squares) and $m_S(T)$ (circles) parameters, with a curve fit (solid line) of the $I_{S0}(T)$–T data to the Richardson–Dushman formula $I_{S0}(T) \propto T^2\exp[-0.11\,\mathrm{eV}/k_BT]$.

Simmons' model for the 'classical' Schottky-type conduction [45–48], according to which the junction current is often described by equation (A2), could be applied to describe the bias/temperature dependence of the measured reverse current of the present heterojunction at reverse-bias voltages above 0.4 V. In the inset to figure 10, one can see a plot of $m_S(T)$ versus $1000/T$, where $m_S(T)$ is the slope of the high-bias linear portions of the semi-log reverse current versus $V^{1/2}$ curves obtained, which can be used to determine the Schottky coefficient β_S ($=(e/4\pi\varepsilon_0\varepsilon_r)^{1/2}$). This plot is reasonably linear over a somewhat extended temperature range up to 230 K, above which a noticeable deviation from this linearity can be noticed, with the values of m_S tending to become less temperature dependent and scattering about a value of 2.4. Using a crude value of $w = 5$ nm, the width of the interfacial depletion region at the presumed pseudo-Schottky contact, a value of $\beta_{S,\,exp} \sim 0.3 \times 10^{-5}\ V^{1/2}\ m^{1/2}$ was estimated, which is in 'roughly good' agreement with the predicted value $\beta_{S,\,theor} = 1.39 \times 10^{-5}\ V^{1/2}\ m^{1/2}$ using $\varepsilon_r = 7.5$ for the rf-MSD B_5C material [2]. Assuming a much larger value for the width of the interfacial depletion region should lead to a less discrepancy between the theoretical and experimental values of β_S, but this is highly unlikely, as the physical width of the polycrystalline B_5C film used does not exceed 60 nm.

Alternatively, the above-observed discrepancy between the theoretically calculated and experimentally deduced values of the Schottky coefficient β_S may be understood if one presumes that the 'classical' Simmons' Schottky-emission conduction model is inappropriate since interface-localized states could exist at the Schottky-like contact. In real rf magnetron sputter deposited B_5C/c-Si heterojunctions,

a B_5C/c-Si pseudo-Schottky interface that accommodates such interface states is highly expected and a large density of 'intrinsic' and 'extrinsic' localized states in these heterojunctions can result from several causes. On one hand, the dangling carbon bonds not fully compensated by hydrogen bonds due to the small amount of hydrogen usually present in rf-MSD B_5C films used in such junctions [2, 3] could give rise to the existence of such interface states. Another possible cause for formation of 'intrinsic' interface states at the junction is the unavoidable lattice mismatch between the semiconducting B_5C film and silicon substrates due to the difference between their lattice constants, crystal structures and thermal expansion coefficients [14–22]. A third possibility for the existence of 'extrinsic' interface states could be due to the poor cleanliness of the B_5C/c-Si interface of these heterojunctions that often results, despite much care usually taken in standard fabrication of these junctions, in a contaminated interfacial layer of these localized states. One should thus revert to modified Schottky-type conduction models that take into account the effect of such interface-localized states at a Schottky-like contact.

The charge transport through such a modified Schottky-like interfacial junction can be described by the so-called Bardeen model [17–19, 28, 29, 33, 34], according to which the bias/temperature dependence of the junction current are expressed by equation (A3). A crude quantitative estimation of the parameters α_S and the modified Schottky constant β_{SC} was obtained as follows. Using $\varepsilon_r = 7.5$, a virtual value for 'impurity' concentration $N \sim 10^{15}\,cm^{-3}$, and a density of interface states $D_s \sim 10^{16}\,eV^{-1}\,cm^{-2}$ in an interfacial layer of thickness $\delta \sim 5$ nm and dielectric constant $\varepsilon_{ir} \sim 4$, one obtains $\alpha_S \sim 8$ nm and $\beta_{SC,\,theor} \sim 0.02\,eV\,V^{-1/2}$. This is comparable with the experimentally deduced value of $\beta_{SC,\,exp} \sim 0.04\,eV\,V^{-1/2}$ deduced from the linear-portion gradient of the m_S versus $1000/T$ plot depicted in the inset to figure 10. The high value of D_s might be justified since, as discussed above, a large density of localized energy states could exist in B_5C/c-Si heterojunctions. The experimentally deduced density of states value of $N_s \sim 10^{17}$–$10^{18}\,eV^{-1}\,cm^{-3}$ from the low-bias current–temperature measurements on a similar heterojunction [3] was used to obtain such a value of D_s for an interfacial layer of thickness $\delta \sim 5$ nm. The high N value used could also be justified by the hypothesis that boron carbide compounds, like other boron-rich solids, exhibit considerable concentrations of 'intrinsic' structural defects due to 'inherent' structural imperfections that are fundamental features of these structures and not due to insufficient preparation methods [11]. In addition, one cannot exclude the contribution of 'native' impurities in the parent B_4C target source used in the fabrication of rf-MSD B_5C films [2].

On the other hand, the pre-exponential current factor $I_{S0}(T)$ can be deduced from the intercept of the high-bias linear portions falling on these isothermal semi-log reverse current versus $V^{1/2}$ plots. The temperature dependence of $I_{S0}(T)$ is depicted on a $\ln I_{S0}T^{-2}$ versus $1/T$ plot (inset to figure 10), where a 'visually good' linear fit of the Richardson–Dushman equation [45, 46] to the I_{S0} data is obtained in the temperature region 140–300 K, with an activation energy $\Phi_{S0} \cong 0.11$ eV. The reasonably good straight-line fit of the $\ln I_{S0}T^{-2}$ versus $1/T$ plot implies that the zero-field Schottky-like barrier height Φ_{S0} remains almost constant in the specified temperature range. Although no definite energy-band structure of the B_5C/c-Si junction is yet known, this small value of Φ_{S0} may sound reasonable for an rf-MSD polycrystalline B_5C/crystalline silicon heterojunction, in which a large density of localized energy states often exists. However, using an effective area of $S \sim 0.07\,cm^2$, the intercept of the semi-log $I_{S0}T^{-2}$ versus $1/T$ plot yields a too unrealistically small value of the effective Richardson constant A^{**} and hence of m^*, the effective mass of the charge carriers in the B_5C semiconductor, which is yet not understood. Nonetheless, the overall bias/temperature dependence of the measured reverse-bias current of the present heterojunction can be well described, at least qualitatively, using Bardeen's model for a modified Schottky-like junction interface.

5. Conclusions

The measured dark forward *I–V–T* curves of an undoped rf-MSD B_5C/p-type c-Si heterojunction were thoroughly examined using the currently existing high-field conduction models, which were found to be described, at least qualitatively, by the Apsley–Hughes non-ohmic VRH conduction model [55] over an extended bias-voltage range (∼0.4–2.7 V) at all temperatures below 260 K. This implies that the high-bias forward junction-like behaviour is probably overbalanced by the bulk conduction in its highly-resistive rf-MSD polycrystalline B_5C counterpart layer, in which a VRH Mott-like $T^{-1/4}$ conduction seems to be highly operable. A noticeable discrepancy between the predictions of the Apsley–Hughes single-particle hopping theory and experimental data at intermediate-/low-bias voltages can be partly related to correlated-hopping transport, which is a characteristic of high-resistivity semiconducting samples. However, in the case of the heterojunction used in this work, one should not neglect the paramount role of the junction-like behaviour in the depletion region at these bias voltages. At high temperatures (>260 K), however, a SCLC model can explain the behaviour of the heterojunction forward-bias current–voltage curves, with the effect of carrier mobility due to thermal lattice scattering being taking into account.

On the other hand, the current conduction mechanisms operating in a junction depletion region should give rise to observed high-bias temperature/bias dependence of the heterojunction reverse current, which has been well described by Schottky-like conduction models such as Bardeen's model for a modified Schottky-like interfacial junction that takes into account the effect of interfacial localized states.

Further dc *I–V–T* measurements on well-prepared undoped/'extrinsically' doped $B_{1-x}C_x$ films of different thicknesses/B-to-C ratios and their silicon-based heterojunctions would give a better insight into the charge transport phenomena operable in them. *In situ* experiments on their *C–V–T* characteristics, ac impedance and photoconductivity will also be invaluable [58, 59].

Acknowledgments

The author sincerely thanks Dr A A Ahmad for supplying the heterojunction used in this study. The author is also

thankful to Dr M Amayreh (Department of Linguistics and Phonetics of the University of Jordan) and Dr Mark English (Department of English of the University of Jordan) for their critical proofreading of the manuscript.

Appendix A. Poole–Frenkel and Schottky-type conduction mechanisms

The physics and mathematical formulation of Poole–Frenkel and Richardson–Schottky effects can be found elsewhere [18, 28, 29, 34, 45–49]. The Poole–Frenkel mechanism usually arises from the electric-field-assisted thermal excitation of charge carriers from charged/neutral traps or impurity sites lying in the energy gap into the semiconductor energy band. The type of trapping centres, trapping/de-trapping mechanism, and the field magnitude and/or its direction with respect to the emission flow of the trapped charge carriers in general govern the Poole–Frenkel current. The Richardson–Schottky effect is often referred to as the field-assisted thermionic emission of charge carriers injected from metal electrodes into the semiconductor over a potential barrier. The current–voltage behaviour for the Richardson–Schottky/'classical' Poole–Frenkel effect can be described by the simple formula

$$I(V,T) = BV^{\gamma}\exp\left[-\frac{e\Phi(V)}{k_{\mathrm{B}}T}\right],$$
$$\Phi(V) = \Phi_0 - n\left(\frac{e\eta}{4\pi\varepsilon_0\varepsilon_{\mathrm{r}}\chi d}\right)^{1/2}V^{1/2}. \tag{A1}$$

The parameter $\Phi(V)$ is a field-dependent activation energy representing a Schottky-barrier height or trapping/donor-site energy in the field, with Φ_0 being its zero-field value, k_{B} is the Boltzmann constant, e is the electronic charge, and ε_0 and ε_{r} are, respectively, the permittivity of free space and optical dielectric constant of the material. An effective film thickness d^*, which is smaller than the physical film thickness d (or the width of the interfacial depletion region w), is sometimes used instead of χd, where the factor χ accounts for any practical electric field non-uniformity in the film due to the accumulation layers at the electrode/junction interface [31–34]. The $V^{1/2}$ pre-factor defined in the $\Phi(V)$ relation is often written as $(\beta_{\mathrm{PF}}/r)(\eta/d^*)^{1/2}$ (Poole–Frenkel effect) or $\beta_{\mathrm{S}}/w^{1/2}$ (Richardson–Schottky effect), where $\beta_{\mathrm{PF}}/\beta_{\mathrm{S}}$ are the Poole–Frenkel/Schottky coefficients defined by $\beta_{\mathrm{PF}} = 2\beta_{\mathrm{S}} = (e/\pi\varepsilon_0\varepsilon_{\mathrm{r}})^{1/2}$ and the compensation factor r can have values from 1 to 2 [22, 45, 46]. Using $\varepsilon_{\mathrm{r}} = 7.5$, theoretical values of $\beta_{\mathrm{S}} = 1.39\times10^{-5}\ \mathrm{V}^{1/2}\,\mathrm{m}^{1/2}$ and $\beta_{\mathrm{PF}} = 2.77\times10^{-5}\ \mathrm{V}^{1/2}\,\mathrm{m}^{1/2}$ are readily obtained. For the Schottky-emission mechanism, $n = \eta = 1$, $\gamma = 0$ and $B = SA^{**}T^2$, where S is the effective contact area and $A^{**} = 1.2\times10^6(m^*/m_0)$ A m^{-2} K^{-2} is the effective Richardson constant, with m^* and m_0 being respectively the carrier effective mass near an energy-band extremity and free-electron mass [28, 29]. The corresponding I–V characteristics are given by the Richardson–Schottky formula [45, 46]

$$I_S(V,T) = I_{S0}\exp\left[\frac{e\beta_S V^{1/2}}{k_{\mathrm{B}}Tw^{1/2}}\right]$$
$$= SA^{**}T^2\exp\left[-\frac{\Phi_0}{k_{\mathrm{B}}T}\right]\exp\left[\frac{e\beta_{\mathrm{S}}V^{1/2}}{k_{\mathrm{B}}Tw^{1/2}}\right]. \tag{A2}$$

The effect of interface states on the bias dependence of a junction reverse current can be accounted for by the use of Bardeen's model, with the Schottky constant β_{SC} being now determined by the depletion-layer charge density N and interface parameters δ, ε_{i} and D_{S} that, respectively, denote its thickness, permittivity and density of states (eV^{-1} m^{-2}) [29, 34]

$$I_{\mathrm{rev}}(V,T) = I_{S0}\exp\left[\frac{\beta_{\mathrm{SC}}V^{1/2}}{k_{\mathrm{B}}T}\right],$$
$$\beta_{\mathrm{SC}} = \alpha_{\mathrm{S}}\left(\frac{2e^3N}{\varepsilon_0\varepsilon_{\mathrm{r}}}\right)^{1/2}, \tag{A3}$$
$$\alpha_{\mathrm{S}} = \frac{\delta\varepsilon_0\varepsilon_{\mathrm{r}}}{\varepsilon_{\mathrm{i}} + e\delta D_{\mathrm{S}}}.$$

For a modified Poole–Frenkel mechanism, $n = 2$, $\eta = 1$ or 2, $\gamma = 1$, $\Phi_0 = E_0$ (zero-field trapping/ionizable centre energy), while the parameter B has in general a variety of forms, depending on temperature, applied field F, material conductivity, trapping/de-trapping (emission) mechanism, field dependence of the trapped charge-carrier emission direction/lifetime or displacement [22, 31–34, 45–49]. Other complex Poole–Frenkel formulae were put forward [20] to describe Poole–Frenkel emission from single-/multiple-ionizable centres, where the current–voltage dependence is described in terms of hyperbolic functions $f_{\mathrm{p}}(\alpha, \sinh\alpha, \cosh\alpha)$, with $\alpha \equiv \beta_{\mathrm{PF}}F^{1/2}/k_{\mathrm{B}}T$, which, at high electric fields, approximate to current–voltage dependence given in equation (A1). In principle, one can follow the $F^{1/2}T^{-1}$ or FT^{-1} normalization techniques to identify the single- or multiple-centre Poole–Frenkel conduction mechanism in a semiconductor sample [20, 54].

Appendix B. SCLC conduction

The applicability of SCLC mechanism requires, at least, one Schottky contact at a metal–semiconductor interface/pseudo-Schottky contact (at the junction interface) for continuous supply of injected charge carriers to sustain space-charge-limited currents in the material [18–21, 29, 34–37, 43, 44]. The SCLC conduction should become important when the density n_{i} of injected free-charge carriers is much larger than the thermal-/light-generated free-charge-carrier density n_0. In general, the space charge formation and the distribution nature of traps in a specimen, which often capture/immobilize the injected charge carriers, are important factors that govern the SCLC mechanism. For single-energy shallow traps of total concentration N_{t} and energy E_{t} below the edge $E_{\mathrm{c}}/E_{\mathrm{v}}$ of conduction/valence energy band, the one-charge carrier SCLC I–V characteristics are often described by a V^2 law (or Mott–Gurney square law) [34–37, 43, 44]

$$I(V,T) = \frac{9}{8}\Theta(T)\varepsilon_0\varepsilon_{\mathrm{r}}\mu_{\mathrm{d}}V^2\frac{S}{d^3},$$
$$\Theta(T) = \frac{n_{\mathrm{f}}}{n_{\mathrm{t}}} = \frac{N_{\mathrm{eff}}}{N_{\mathrm{t}}}\exp\left[-\frac{E_{\mathrm{t}}}{k_{\mathrm{B}}T}\right]. \tag{B1}$$

Herein, μ_{d} is the charge-carrier drift mobility, the function $\Theta(T)$ ($\ll1$) is the ratio of free injected and initial charge carrier density n_{f} to trapped carrier density n_{t}, and $N_{\mathrm{eff}} = 4.83\times10^{21}(m^*/m_0)^{3/2}T^{3/2}$ (SI units) is the effective

density of states in the band. One can thus write the SCLC V^2 law in the form

$$I(V,T) = 4.78 \times 10^{10} \left(\frac{m^*}{m_0}\right)^{3/2} \times \left[\frac{S\varepsilon_r \mu T^{3/2}}{N_t d^3} \exp\left(-\frac{E_t}{k_B T}\right)\right] V^2. \quad \text{(B2)}$$

In the case of a uniform density of traps per unit energy $N_t(E)$ ($=N_n$), as in some disordered materials rich in imperfections and defect centres, the one-carrier SCLC *I–V* behaviour can be described by [43, 44]

$$I(V,T) = 2en_0\mu \left(\frac{V}{d}\right) \exp\left[\left(\frac{2\varepsilon_0\varepsilon_r}{eN_n d^2 k_B T}\right) V\right]. \quad \text{(B3)}$$

Further, for energetically exponentially distributed traps that are usually characterized by a temperature parameter T_c [34–37, 43, 44], the SCLC current–voltage relation is often written as

$$I_{SCLC}(V,T) = SeN_{eff}\mu \left(\frac{\varepsilon_0\varepsilon_r}{eN_t}\right)^{\ell} \left(\frac{V^{\ell+1}}{d^{2\ell+1}}\right) = K(T)V^{m(T)}, \quad \text{(B4)}$$

$$K(T) = C \exp\left(-\frac{E_X}{k_B T}\right),$$

where $\ell = T_c/T \equiv m(T) - 1$. For $T_c > T$, $m(T) > 2$, while when $T_c < T$, $\ell \sim 1$ and equation (B4) reduces to the Mott–Gurney square law $I_{SCLC}(V) \propto V^2/d^3$. E_X is an activation energy that defines a finite Fermi level with free-charge carriers being emitted from low-lying filled traps below this Fermi level to the energy band involved.

Appendix C. Thermally-assisted hopping transport phenomena in the ohmic and non-ohmic regimes

The low-temperature current transport with too low activation energies (few meV) is usually related to hopping of charge carriers between localized energy states close to the Fermi level E_F within the energy gap of the material [20–23, 49–57]. Different theoretical approaches were in general employed to obtain a variety of formulae that describe hopping charge transport conduction in semiconducting materials, which are generally determined by the distribution nature of localized states, interactions between localized charge carriers, specimen dimension, temperature range and strength of the applied electric field [11–13, 20, 49–56]. Generally speaking, these hopping conduction models yield a low-temperature dependence for dc conductivity $\sigma_{dc}(T)$ at very low electric fields (ohmic regime) of the form $\ln \sigma_{dc}(T) \propto T^{-1/n}$, with $n = 2, 3, 4, 7$ [20, 32, 49–56]. The so-called Efros' $T^{-1/2}$ dependence describes hopping conduction with Coulombic interactions between localized charge carriers that lead to the creation of a soft gap in the density of states at E_F. The conductivity behaviour with $n = 3$ is often related to hopping conduction in two-dimensional structures, which is affected by the specimen thickness/surface conditions [22, 32, 49, 50]. However, a different conductance $T^{-1/3}$ dependence is often employed to describe thermally-assisted tunnelling due to a bulk ionizable-centre emission process, with the centre barrier being reduced by the applied electric field (Poole–Frenkel effect) into a quasi-conduction band, in terms of a closed-form analytical expression [20]

$$\left.\begin{aligned} \ln I(F,T) &\propto -\frac{2^{4/3}E_p^{4/3}D^{2/3}}{(k_B T)^{1/3}} \times \left\{1 - 2^{-2/3}D^{2/3}E_p^{1/3}(k_B T)^{2/3}\right\} \\ &\propto -\frac{2E_0}{k_B T}\left(1 - \frac{E_0}{2E_p}\right) \\ E_p &= E_i - \beta_{PF}F^{1/2}, \qquad D = \tfrac{4\pi}{h}\tfrac{m^{1/2}}{eF}, \\ E_0 &= (Dk_B T)^{2/3}\, 2^{1/3}\, E_p^{4/3}. \end{aligned}\right\} \quad \text{(C1)}$$

Herein, E_i is the zero-field ionization energy, E_p is the peak energy of the reduced Poole–Frenkel barrier, E_0 ($<E_p$) is the energy at which tunnelling occurs and h is Planck's constant. For low fields, E_0 approaches E_p and there is a critical field, below which E_0 becomes constant and a thermally-activated behaviour occurs.

The case with $n = 1/4$, often known as the variable-range-hopping (VRH) Mott's law, describes hopping conduction in three-dimensional (3D) systems for a constant (flat) density of localized impurity energy states, $g(E_F)$ with the ohmic $\sigma_{dc}(T)$ being described by [32, 49–57]

$$\sigma(T) = e^2 \nu_{ph} f\,(g(E_F), \alpha)\, T^{\ell} \exp\left[-\left(\frac{T_M}{T}\right)^{1/4}\right], \qquad T_M = \lambda\alpha^3/k_B g(E_F), \quad \text{(C2)}$$

where ν_{ph} is a frequency parameter, T_M (Mott's localization temperature) is a measure of the material amorphosity/crystallinity, $\lambda = 10$–57 [49, 57] and $l = 2$, $-1/2$ or $-1/4$ [49–56]. Different forms of the function $f\{g(E_F), \alpha\}$, in terms of $g(E_F)$ and the decay constant α of localized-state wavefunctions, were also obtained [49–56]. Charge carriers can also jump among localized empty neutral centres (traps) and give rise to the so-called 'trap hopping' current of a $T^{-1/4}$ dependence, while for hopping of charge carriers from ionizable centres into traps (hybrid case), a $T^{-1/7}$ behaviour of conductance is expected [20].

The mathematical formalism tackling the problem of hopping conduction phenomena at electric fields beyond the ohmic region is in general too complex and diverse. Nonetheless, only few stringent analytically tractable expressions describing non-ohmic hopping conductivity in semiconducting materials are available [20, 49–56]. In general, the theoretical models of hopping conduction in the presence of electric field often separate, using different criteria, the conductivity behaviour into ohmic at low fields and non-ohmic at moderate, high and very high electric fields [49–56]. A practical criterion often utilized to categorize the strength of the applied electric field F is via a parameter $\beta = eF/2\alpha k_B T$, with the ohmic regime being characterized by $\beta \ll 1$ and the region of very high fields corresponds to $\beta \gg 1$. All these hopping conduction models give a low-field conductivity described by a Mott-like $T^{-1/4}$ law for a flat density of localized states, but yielding different non-ohmic field-dependent hopping conductivity formulae [49–56].

Using a Mott-type analysis of hopping conduction, Hill [20] derived analytical formulae to describe the 'trap hopping' current in a semiconductor at low ($\beta < 1$) and high ($\beta > 1$)

fields (equations (C3) and (C4), respectively) for the case of localized trap states with flat density per unit energy N_i

$$\left.\begin{aligned} I(V,T) &\propto T^2 \sinh\left\{1.03eF(\alpha\pi N_i)^{-1/4} \right. \\ &\left. \times (k_B T)^{-5/4}\right\} \exp\left(-\tfrac{C}{T^{1/4}}\right) \\ C &= 2.31\left[\tfrac{2\alpha^3}{\pi k_B N_i}\right]^{1/4} \end{aligned}\right\}. \tag{C3}$$

$$I(V,T) \propto T^2 \exp\left\{-\left[2.31\left(\frac{2\alpha^3}{\pi k_B N_i T}\right)^{1/4} \times \left(1-\frac{eF}{2\alpha k_B T}\right)^{3/4}\right]\right\}. \tag{C4}$$

Other theoretical non-ohmic current expressions of the form $I(V,T) \propto \exp[\varphi F T^{-1/n}]$ were obtained using more complex treatments [51–53] for $g(E_F)$ = constant under moderate electric-field conditions, with different φ- and n-numerical values. Equation (C3) and the analogous current formula derived for exponential distribution of traps [20] reduce to a Mott-like formula at very low fields, implying that the low-field $T^{-1/4}$ law is valid irrespective of the actual trap distribution, about which one can only obtain information from the *I–V* characteristics in high-field regions. One can implement specific procedures that utilize plots of normalized current and field parameters to characterize 'trap hopping' conduction mechanism in a system [20]. In the case of $g(E_F)$ = constant, the normalized current $T^{-1/4}\ln(IT^{-2})$ versus $FT^{-1{\cdot}25}$ plots are often used, whereas for the exponential distribution of traps, plots of $T^{-1/4}\ln(IT^{-2})$ versus $F^2T^{-1/2}$ are usually constructed. An alternative procedure is to examine the field dependence of the gradient $G(F)$ of the plots of $\ln(IT^{-2})$ against $T^{-1/4}$, which can be described, for a 'trap hopping' conduction in a constant distribution of localized traps, by the relation [20]

$$1-\left[\frac{G(F)}{G_0}\right]^{4/3} = \frac{eF}{2\alpha k_B T}. \tag{C5}$$

In the ohmic regime, this gradient should be constant (=G_0). A less informative formula describing $G(F)$ for 'trap hopping' conduction in an energy band of exponentially distributed localized traps is also given [20].

More generally, Apsley and Hughes [55] have advanced a theoretically comprehensive hopping conduction model to describe charge-carrier hopping between randomly distributed localized states of hydrogen-like wavefunctions for any form of density of localized energy states $N(E)$ without using Mott-like optimization arguments [20, 49–52]. In fact, one should implement numerical techniques to evaluate the temperature/field dependence of hopping conductivity of the general Apsley–Hughes hopping conduction model. However, for a constant density of states N, this theory depicts a single analytical expression that describes dc hopping conductivity $\sigma(F, T)$ as a function of electric field F and ambient temperature T

$$\sigma(\beta,T) = M(\beta)\left(\frac{Nk_BTe\nu_{ph}}{2\alpha F}\right)\left(1+\frac{P+Q}{P+1}\right) \times \left(\frac{2}{K(P+Q)}\right)^{1/4} \exp\left[-\left(\frac{2}{K(P+Q)}\right)^{1/4}\right]. \tag{C6a}$$

Herein, the parameters K, P, Q, β and $M(\beta)$ in equation (C6*a*) are expressed by

$$\left.\begin{aligned} \beta &= \tfrac{eF}{2\alpha k_B T}, & Q &= \tfrac{3\beta}{2}+1, \\ K &= \tfrac{N\pi k_B T}{24\alpha^3}, & P &= \tfrac{1+\frac{\beta}{2}}{(1+\beta)^2}, \\ M(\beta) &= -\frac{\frac{3+\beta}{24(1+\beta)^3}-\frac{1}{8}-\frac{\beta}{3}}{\frac{2+\beta}{6(1+\beta)^2}+\frac{1}{3}+\frac{\beta}{2}}. \end{aligned}\right\} \tag{C6b}$$

In the limits of small and large β values, one can greatly simplify the above general Apsley–Hughes hopping-conductivity expression. This expression reduces to Mott's VRH $T^{-1/4}$ relation for too small values of β ($\leqslant$0.1) and for $0.1 < \beta \leqslant 0.5$ to the form

$$\sigma(F,T) \cong \left(\frac{Ne^2\nu_{ph}}{2\alpha^2}\right)\left[\frac{24\alpha^3}{N\pi k_B}\right]^{1/4} T^{-1/4} \times \exp\left\{-\left(1-\frac{\beta^2}{4}\right)\left[\frac{24\alpha^3}{N\pi k_B}\right]^{1/4} T^{-1/4}\right\}. \tag{C7}$$

For $\beta \geqslant 10$, however, the Apsley–Hughes $\sigma(F, T)$ expression yields, as reported by others [49–53], a temperature-independent conductivity with a rather strong electric-field dependence of the form

$$\sigma(F,T) \to \sigma(F) = \left(\frac{Ne^2\nu_{ph}}{4\alpha^2}\right)\left[\frac{64\alpha^4}{e\pi N}\right]^{1/4} \times F^{-1/4}\exp\left\{-\left[\frac{64\alpha^4}{N\pi e}\right]^{1/4} F^{-1/4}\right\}. \tag{C8}$$

References

[1] Jankowski A, Makowiecki D and Mckeman M 1989 *J. Appl. Phys.* **65** 4450

[2] Ahmad A A 1996 Deposition and characterization of boron carbides *PhD Thesis* (Lincoln: University of Nebraska)
Ahmad A A, Ianno N J, Hwang S D and Dowben P A 1998 *Thin Solid Films* **335** 174

[3] Abdul-Gader M M, Al-Binni U A, Ahmad A A, Al-Basha M A and Ianno N J 2001 *Int. J. Electron.* **88** 873

[4] Ahmad A A, Ianno N J, Synder P G, Welipitiya D, Byun D and Dowben P A 1996 *J. Appl. Phys.* **79** 8643

[5] Lee S W, Mazurowski J, Ramseyer G and Dowben P A 1992 *J. Appl. Phys.* **72** 4925
Lee S W, Mazurowski J, O'Brian Q Y, Tia J J, Callcott Y, Tan Y, Miyano K E, Ederer D L, Mueller D R and Dowben P A 1993 *J. Appl. Phys.* **74** 6919

[6] Perkins F K, Onellion M, Lee S W, Li D Q, Mazurowski J and Dowben P A 1992 *Appl. Phys.* A **54** 442

[7] Byun D, Hwang S D, Dowben P A, Perkins F K, Filips F and Ianno N J 1994 *Appl. Phys. Lett.* **64** 1968
Hwang S D, Byun D, Ianno N J and Dowben P A 1996 *Appl. Phys. Lett.* **68** 1495
Mcllroy D N, Hwang S D, Yang K, Remmes N, Dowben P A, Ahmad A A, Ianno N J, Li J Z, Lin J Y and Jiang H X 1997 *Appl. Phys.* A **67** 335
Hwang S D, Yang K, Dowben P A, Ahmad A A, Ianno N J, Li J Z, Lin J Y, Jiang H X and Mcllroy D N 1997 *Appl. Phys. Lett.* **70** 1028

[8] Chen H Y, Wang J, Yang H, Li W Z and Li H D 2000 *Surf. Coat. Technol.* **128** 329
Reigada D C, Prioli R, Jacobsohn L G and Freire F L 2000 *Diam. Relat. Mater.* **9** 489

[9] Armstrong D R, Bolland J, Perkins P G, Will G and Kirfel A 1983 *Acta Crystallogr.* B **39** 324

[10] Bylander D M, Kleinman L and Lee S 1991 *Phys. Rev.* B **42** 1394

[11] Werheit H, Kuhlmann U, Laux M and Lundstrom T 1993 *Phys. Status Solidi* b **179** 489
Kuhlmann U, Werheit H, Pelloth J, Keune W and Lundstrom T 1995 *Phys. Status Solidi* b **187** 43
Schmechel R and Werheit H 1999 *J. Phys.: Condens. Matter* **11** 6803

[12] Emin D 1974 *Phys. Rev. Lett.* **32** 303
Wood C and Emin D 1984 *Phys. Rev.* B **29** 4582
Aselage T L, Emin D and McCready S S 2000 *Phys. Status Solidi* b **218** 255
Samara G A, Tardy H L, Venturini E L, Aselage T L and Emin D 1991 *Proc. 10th Int. Symp. on Boron Carbides and Related Compounds* (New York: AIP) p 77

[13] Zuppiroli L and Forro L 1989 *Phys. Lett.* A **141** 181
Zuppiroli L, Papandreou N and Kormann R 1991 *J. Appl. Phys.* **70** 246
Papandreou N and Zuppiroli L 1991 *Proc. 10th Int. Symp. on Boron Carbides and Related Compounds* (New York: AIP) p 85

[14] Akkal B, Benamara Z, Bideux L and Gruzza B 1999 *Semicond. Sci. Technol.* **14** 266

[15] Singh A, Reinhardt K C and Anderson W A 1992 *J. Appl. Phys.* **71** 4788

[16] Yoo J, Fahrenbruch A L and Bube R H 1990 *J. Appl. Phys.* **68** 4694
Peters M G, Fahrenbruch A L and Bube R H 1988 *J. Appl. Phys.* **64** 15
Fahrenbruch A L Private communication

[17] Milnes A G and Feucht D L 1972 *Heterojunctions and Metal-Semiconductor Junctions* (New York: Academic)

[18] Sharma B L and Purohit R K 1974 *Semiconductor Heterojunctions* (Oxford: Pergamon)
Sharma B L (ed) 1984 *Metal-Semiconductor Schottky Barrier Junctions and their Applications* (London: Plenum)

[19] Frost S R 1987 *Heterojunction Band Discontinuities—Physics and Device Applications* ed F Capasso and G Margaritondo (Amsterdam: North-Holland) p 359

[20] Hill R M 1971 *Thin Solid Films* **7** 224
Hill R M 1971 *Thin Solid Films* **7** R57
Hill R M 1973 *Thin Solid Films* **15** 369
Hill R M 1971 *Phil. Mag.* **23** 59
Hill R M 1971 *Phil. Mag.* **24** 1307

[21] Baranyuk V E and Makhnii V P 1991 *Sov. Phys.–Semicond.* **25** 130

[22] Staryga E and Swiatek J 1979 *Thin Solid Films* **56** 311
Swiatek J 1976 *Phys. Status Solidi* a **38** 285

[23] Kireev P S 1975 *Semiconductor Physics* (Moscow: Mir)

[24] Khan M R H, Detchprohm T, Hacke P, Hiramatsu K and Sawaki N 1995 *J. Phys. D: Appl. Phys.* **28** 1169

[25] Dos Santos O, Mathet V, Fau C, Charar S, Collot P, Nguyen-Van-Dau F and Obadi A 1995 *Phys. Status Solidi* a **148** 475

[26] Hernández M P, Alonso C F, Martel A, Casielles E, Rejón V and Peña J L 2000 *Phys. Status Solidi* b **220** 209
Hernández M P, Alonso C F and Peña J L 2000 *Phys. Status Solidi* b **220** 789

[27] Werner J H 1988 *Appl. Phys.* A **47** 291
Lee T C, Fung S, Beling C D and Au H L 1992 *J. Appl. Phys.* **72** 4739
Norde H 1979 *J. Appl. Phys.* **50** 5052
Chot T 1981 *Phys. Status Solidi* a **66** K43
Cibils R M and Buitrago R H 1985 *J. Appl. Phys.* **58** 1072
Bohlin K E 1986 *J. Appl. Phys.* **60** 1223
Manifacier J C, Brortyb N, Ardebili R and Charles J P 1988 *J. Appl. Phys.* **64** 2502

[28] Shur M 1990 *Physics of Semiconductor Devices* (Englewood Cliffs, NJ: Prentice-Hall)
Sze S M 1981 *Physics of Semiconductor Devices* 2nd edn (New York: Wiley)

[29] Rhoderick E H 1978 *Metal Semiconductor Contacts* (Oxford: Clarendon)
Rhoderick E H and Williams R H 1988 *Metal Semiconductor Contacts* 2nd edn (Oxford: Clarendon)

[30] Ercelebi C, Brinkman A W, Furlong T S and Woods J 1990 *J. Cryst. Growth* **101** 162
Simmons M Y, Al-Allak H M, Brinkman A W and Durose K 1992 *J. Cryst. Growth* **117** 959
Al-Allak H M, Brinkman A W, Richter H and Bonnet D 1996 *J. Cryst. Growth* **159** 910

[31] Mathew X, Enriquez J P, Sebastian P J, Pattabi M, Sanchez-Juarez A, Campos J, McClure J C and Singh V P 2000 *Solar Energy Mater. Sol. Cells* **63** 355
Anthone S 1993 *Phys. Status Solidi* a **136** 401

[32] Nguyen T P, Tran V H and Massardier V 1993 *J. Phys.: Condens. Matter* **5** 6243

[33] Rahman A S Md S and Hogarth C A 1986 *J. Mater. Sci. Lett.* **5** 693
Buchwald W R and Johnson N M 1988 *J. Appl. Phys.* **64** 958

[34] Rakhshani A E, Makdisi Y, Mathew X and Mathews N R 1998 *Phys. Status Solidi* a **168** 177
Rakhshani A E 1991 *J. Appl. Phys.* **69** 2365
Rakhshani A E 1991 *J. Appl. Phys.* **69** 2290
Rakhshani A E, Makdisi Y and Mathew X 1997 *J. Mater. Sci. Mater. Electron.* **8** 207

[35] Smid V, Mares J J, Stourac L and Kristofik J 1985 *Tetraherally Bonded Amorphous Semiconductors* ed D Adler and H Frizche (New York: Plenum) p 483

[36] Dunn B and Mackénzie J D 1976 *J. Appl. Phys.* **47** 1010

[37] Marsal L F, Pallarès J, Correig X, Calderer J and Alcubilla R 1996 *J. Appl. Phys.* **79** 8493

[38] Cowan G 1998 *Statistical Data Analysis* (Oxford: Clarendon)

[39] Garcia A L 1994 *Numerical Methods for Physics* (London: Prentice-Hall)

[40] Mathews J H 1992 *Numerical Methods for Mathematics, Science, and Engineering* 2nd edn (London: Prentice-Hall)

[41] Press W H, Teukolsky S A, Vetterling W T and Flannery B P 1992 *Numerical Recipes in Fortran* 2nd edn (Cambridge: Cambridge University Press)

[42] Loehle G 2001 *Global Non-Linear Optimization using Mathematica* (IL: Loehle Enterprises) version 4.1

[43] Rose A 1955 *Phys. Rev.* **97** 1538

[44] Lambert M A and Mark P 1970 *Current Injection in Solids* (New York: Academic)

[45] Yeargan J R and Taylor H L 1968 *J. Appl. Phys.* **39** 5600

[46] Simmons J G 1967 *Phys. Rev.* **155** 657
Simmons J G 1968 *Phys. Rev.* **166** 912
Simmons J G 1971 *J. Phys. D: Appl. Phys.* **4** 613
Simmons J G 1970 *Handbook of Thin Film Technology* ed L I Maissel and R Glang (New York: McGraw-Hill) ch 14

[47] Jonscher A K 1967 *Thin Solid Films* **1** 213
Jonscher A K and Ansari A 1971 *Phil. Mag.* **23** 205

[48] McClean I P and Thomas C B 1992 *J. Appl. Phys.* **72** 4749

[49] Mott N F and Davis E A 1979 *Electronic Processes in Non-Crystalline Materials* 2nd edn (Oxford: Clarendon)
Nagels P 1979 *Amorphous Semiconductors* ed M H Brodsky (New York: Springer) p 113
Botteger H and Bryskin V V 1985 *Hopping Conduction in Solids* (GDR: VCH)

[50] Shklovskii B I and Efros A L 1984 *Electronic Properties of Doped Semiconductors* (New York: Springer)
Efros A L and Shklovskii B I 1985 *Electron-electron Interaction in Disordered Systems* ed A L Efros and M Pollak (Amsterdam: North-Holland) p 409

[51] Shklovskii B I 1973 *Sov. Phys.–Semicond.* **6** 1053
Shklovskii B I 1973 *Sov. Phys.–Semicond.* **6** 1964
Shklovskii B I 1976 *Sov. Phys.–Semicond.* **10** 855

[52] Pollak M and Riess I 1976 *J. Phys. C: Solid State Phys.* **9** 2339
[53] Grannan S M, Lange A E, Haller E E and Beeman J W 1992 *Phys. Rev.* B **45** 4516
[54] Morgan M and Walley P A 1971 *Phil. Mag.* **23** 661
[55] Apsley N and Hughes H P 1974 *Phil. Mag.* **30** 963
Apsley N and Hughes H P 1975 *Phil. Mag.* **31** 1327
[56] Dallacasa V, Paracchini C and De Stabile S 1988 *J. Phys. C: Solid State Phys.* **21** L567
Dallacasa V 1986 *J. Phys. C: Solid State Phys.* **19** L485
[57] Abdul-Gader M M, Al-Basha M A and Wishah K A 1998 *Int. J. Electron.* **85** 21
[58] Palinginis K C, Lubianiker Y, Cohen J D, llie A, Kleinsorge B and Milne W I 1999 *Appl. Phys.* **74** 371
[59] Marée C H M, Roosendaal S J, Savenije T J, Schropp R E I, Schaafsma T J and Habraken F H P M 1996 *J. Appl. Phys.* **80** 3381